NUCL SCI TECH (2018) 29:17
https://doi.org/10.1007/s41365-018-0358-4

B_4C/NRL flexible films for thermal neutron shielding

Yi-Chuan Liao[1] · Dui-Gong Xu[1] · Peng-Cheng Zhang[2]

Received: 2 April 2017 / Revised: 4 May 2017 / Accepted: 9 May 2017 / Published online: 25 January 2018

Abstract Boron carbide/natural rubber latex (B_4C/NRL) flexible films were prepared via dip-molding with B_4C content in the range of 5–55 wt% for thermal neutron (0.0253 eV) shielding. B_4C was well dispersed in NRL according to microscopic observation. Both the inside and outside surfaces of the film were smooth. For B_4C/NRL flexible films, the minimum elongation at break was greater than 600%, the minimum tensile strength was greater than 12 MPa, and the hardness was in the range of 35–55 HA, which were suitable for preparing flexible wearable products. The attenuation efficiencies of the B_4C/NRL flexible films for thermal neutrons were also calculated. The B_4C/NRL flexible films exhibit good attenuation effect for thermal neutrons.

Keywords B_4C · Natural rubber latex · Thermal neutron · Shield · Flexible film

1 Introduction

Radioactive rays and related radioactive nuclides have been widely employed in industries. Although radioactive rays provide significant benefits to mankind, they are harmful to human health if appropriate shielding is not employed [1, 2]. Neutrons have a wide range of applications [3, 4]; however, neutron shielding is a challenging work owing to its high radiobiological effect, significant dose weighting factors, and strong penetration abilities [5]. Appropriate protection must be implemented to ensure the health and safety of handlers. A series of materials were investigated to shield against neutrons of different energies [6–8].

In order to avoid the radiation harm caused by thermal neutrons, low Z elements have been commonly used for shielding against thermal neutrons [9]. For example, the investigation by Iskender Akkurt et al. [6] suggested that the boronizing process improved the radiation shielding properties of austenitic stainless steel. The thermal neutron absorption cross-section of B_4C is 760 barn (1 barn = 10^{-24} cm^2) [10], which is suitable for shielding against thermal neutrons. Moreover, traditional structural materials containing B_4C such as metals [11, 12], ceramics [13, 14], concrete [15–17], and polymers [18] have been widely used in neutron shielding owing to their mechanical and chemical stability, abundance, and non-toxicity.

A flexible material in the form of protective shades, protective clothing, protective gloves, and protective helmets is required to shield against neutrons. However, traditional structural materials such as metals, ceramics, concrete, and polymer sheets cannot satisfy these flexible requirements. Therefore, many attempts have been made to develop flexible materials. For example, Hao et al. [19]

This work was supported by the National Natural Science Foundation of China (No. 11405149) and the Sichuan Academic and Technical Leader Program (No. DTR201501).

✉ Peng-Cheng Zhang
zpc113@sohu.com

[1] Institute of Materials, China Academy of Engineering Physics, Jiangyou 621907, China

[2] Science and Technology on Surface Physics and Chemistry Laboratory, Jiangyou 621908, China

prepared a flexible, flame-retardant composite using a high-functional methyl vinyl silicone rubber matrix with B_4C as the neutron absorber. Mersin University prepared ethylene propylene diene monomer (EPDM) rubber with boric acid for neutron shielding [20, 21]. Gwaily et al. [22, 23] prepared B_4C/NR composites as thermal neutron radiation shields. Ninyong et al. [24] investigated natural rubber (NR) with the addition of boron oxide and boric acid for potential use as a flexible shielding material. In their studies, the preparation of raw materials and methods was aimed at obtaining solid rubber. There are significant differences between solid rubber and rubber latex, such as the preparation method, properties of the product, and applications. Rubber latex, especially natural rubber latex (NRL), is widely used in daily life as a traditional flexible material and can be molded into an arbitrary shape with good plasticity and elasticity. Few works have been reported on NRL as a matrix to shield against thermal neutrons.

In this study, NRL and B_4C were selected as the matrix and attenuation material, respectively. B_4C was pre-treated using ball milling to enhance its dispersity and stability in NRL. B_4C/NRL flexible films with B_4C content in the range of 5–55 wt% were prepared via dip-molding and were deemed suitable for wearable products. The mechanical properties and thermal neutron shielding properties of the B_4C/NRL flexible films were analyzed.

2 Experimental

2.1 Preparation of B_4C dispersion

The purity of B_4C (Mudanjiang Qianjin Boron Carbide Co., Ltd) was greater than 99.99%. Commercially available B_4C powders (3.6 μm, 2.45 g cm^{-3}) were pre-treated using ball milling at 300 rpm for 12 h. The mass ratio of the corundum ball and material was 2:1. The mass ratio of different diameters of corundum balls was $\phi20{:}\phi10{:}\phi6 = 1{:}3{:}6$. All the other chemicals and analytical reagents were used as received. The B_4C dispersion consisted of B_4C, distilled water, ammonia (analytical reagent (AR), Aladdin), and dispersant (two nekal, BX, Aladdin) with a mass ratio of 1:1:0.5:0.01. Ammonia was used to adjust the pH value to enhance the stabilization of the B_4C dispersion. The dispersant BX was used to increase the wettability of the B_4C particles and to prevent the re-agglomeration and settlement of B_4C particles.

2.2 Preparation of pre-vulcanization NRL

The pre-vulcanization composition of the NRL is provided in Table 1. All the chemicals and analytical reagents were used as received. The compounding agent included vulcanizater (S, AR, Aladdin), active agent (ZnO, AR, Aladdin), accelerator (zinc diethyl dithiocarbamate, AR, Aladdin), antioxidant (*D*,*N*-phenyl-2-naphthylamine, AR, Aladdin), and dispersant BX [25]. The mass ratio of the compounding agents and distilled water was 1:1.5. The compounding agent dispersion was prepared via milling at 300 rpm for 12 h. The pre-vulcanized latex consisted of NRL (60 wt% DRC HA, TVRTEX, Thailand, 60 mPa s), compounding agent dispersion, KOH (AR, Aladdin), casein (AR, Aladdin), and Peregal O (leveling Agent O, polyoxyethylene alkyl ether). The compounding agent dispersion was slowly added to NRL by stirring. Subsequently, the solution of KOH, casein, and Peregal O was mixed into NRL. The viscosity of NRL was controlled by adjusting the compounding agent. After curing at 60 °C for 1 h and thereafter cooling to room temperature (25 °C), the pre-vulcanized NRL was ready to use.

2.3 Preparation of B_4C/NRL flexible films

The B_4C dispersion was added and dispersed into the pre-vulcanized NRL by stirring. After 48 h, filtration and defoaming were performed to obtain the desired latex (5–55 wt% B_4C/NRL). The proper viscosity of the B_4C/NRL mixture used for dip-molding was 60–100 mPa s.

The B_4C/NRL flexible films were prepared using dip-molding. Ceramic plates or molds were dipped in NRL for several seconds and thereafter allowed to set. After drying, the molds were vulcanized by boiling water and dried in an oven. Subsequently, the B_4C/NRL flexible films were ready for thermal neutron shielding.

The thickness of the film can be controlled by dipping multiple times. After a single dip, the thickness of the film ranged from 0.1 to 0.35 mm. The molds were dipped multiple times to achieve the desired thicker films.

2.4 Properties characterization

The viscosity of the latex was measured using a digital viscometer (NDJ-5S, Shanghai Ping Xuan Scientific Instrument Co., Ltd) at room temperature. The median diameter (D_{50}) of B_4C was detected using a laser particle size analyzer (Mastersizer 2000) at a scanning speed of 1000 times/s with deionized water as the dispersing agent. The dispersion state of B_4C in NRL was analyzed using a scanning electron microscope (SEM, JSM6390 LV, Japan JEOL) and an energy dispersive spectrometer (EDS). Fourier transform infrared (FT-IR) spectra were recorded using Nicolet FT-IR Nexus, in the range of 4000–500 cm^{-1}. The test mode was set to total reflection. Wide-angle X-ray diffraction (WAXD) was performed on a D/Max-RB target X-ray diffraction (Japan Rigaku) under

Table 1 Dry weight composition of pre-vulcanized NRL

Raw material	NRL	S	ZnO	ZDC	D	Casein	Peregal O	KOH	BX
Content (wt%)	100	1	1	1	0.2	0.1–0.5	0.1–0.5	0.1–0.2	0.1

the following condition: Cu Kα radiation (λ = 0.15406 nm) at the voltage of 40 kV. The scanning rate was 15°/min in the angle range of 10°–80°. Mechanical properties of the films including the tensile strength and elongation at break were tested using a universal testing machine (CMT6103, Meitesi Industry System (China) Co. Ltd). The harnesses of the films were measured using a shore durometer (LX-A, China Jun Ping Machinery Factory).

2.5 Thermal neutron shielding property measurement

The thermal neutron shielding property of the films was evaluated using a 49-2 swimming-pool-type reactor at the Reactor Engineering Research and Design Institute of the Chinese Atomic Energy Academy. The power of the 49-2 reactor was 3500 MW, with light water used as the coolant and moderator. Figure 1 illustrates a schematic diagram of the thermal neutron shielding assessment.

During the measurement, the sample was placed 1600 mm from the thermal column. Three Dy–Al alloy foil detectors were placed on both sides of each sample. The positions of the six foil detectors on both sides of the sample did not overlap. A cadmium foil was used for shielding against lateral neutrons of the thermal column. The diameter of Dy–Al alloy foil was 4 mm with a thickness of 0.3 mm. The performances of Dy–Al alloy foil detectors were as follows: The correction coefficient between the foil detectors was less than 1%, and the Dy detector was only sensitive to thermal neutrons.

Cadmium was used to absorb thermal neutrons, and a small collimator aperture was used to reduce the counting rate. A 3-cm lead brick was used to screen the γ-rays to reduce their impact. The activation cross-section of the neutrons above the thermal neutrons was very small and could be ignored relative to the thermal neutron activation cross-section. The most probable energy of the thermal neutron was 0.0253 eV. The activity of the foil detector after activation by the neutrons was proportional to the neutron flux rate on the detector. The normalization activity differences between the front and back Dy detectors reflected the thermal neutron shielding performance of the sample. The radioactive decay equation is as follows [16, 17]:

$$A_0 = A \cdot e^{\frac{\ln 2}{T_{1/2}} \cdot t}, \quad (1)$$

where A_0 is the initial normalization activity, A is the normalization activity at time t, and $T_{1/2}$ is half-time.

The thermal neutron shielding performance of the sample was calculated using the following equation:

$$\text{Shielding efficiency} = (A_{\text{front}} - A_{\text{back}})/A_{\text{front}} \times 100\%, \quad (2)$$

where A_{front} and A_{back} represent the normalization activity of the front and back Dy detectors at time t, respectively.

After A_{front} and A_{back} are obtained, the macroscopic cross-section of the actual material was calculated using Lambert–Beer law (3) [7, 26]:

$$A_{\text{back}} = A_{\text{front}} e^{-\sigma \cdot d}, \quad (3)$$

where d is the thickness of the material and σ is the macroscopic cross-section of the material. The term σ was obtained by measuring A_{front}, A_{back}, and d.

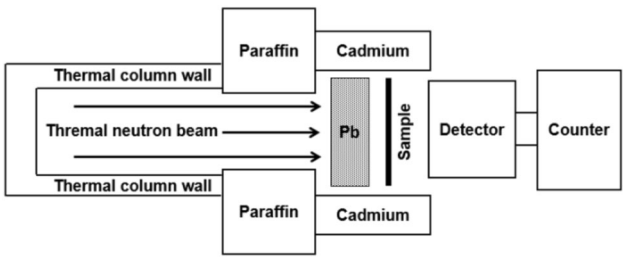

Fig. 1 Schematic diagram of the thermal neutron shielding assessment

3 Results and discussion

3.1 Dispersion state of B_4C in NRL

Particles in commercial B_4C powders agglomerate owing to environmental humidity. The B_4C used was pretreated via ball milling to avoid particle agglomeration and precipitation. The median diameter (D_{50}) of B_4C varied with the milling time, which was detected using a laser particle size analyzer. As shown in Fig. 2, D_{50} of the B_4C particles reduced from 3.6 to 1 μm after milling for 12 h. The granule shape of the B_4C particles did not change after milling. No apparent precipitation was observed after 10 days, indicating that the stability of the pre-vulcanized latex containing B_4C is suitable for practical applications.

The SEM images of the flexible film with different contents of B_4C are shown in Fig. 3. The bright spots in the

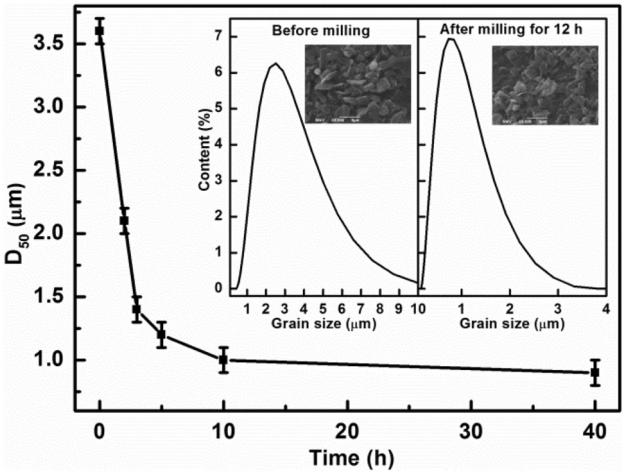

Fig. 2 Median diameter (D_{50}) of B_4C particles with milling time. Inset images: grain size distribution and SEM images of B_4C particles (*a*) before milling and (*b*) after milling for 12 h

figure are the B_4C particles. The small pits are the trails left behind when B_4C particles peeled off the interface. B_4C particles are well distributed in NRL with no pores or cracks.

Figure 4 demonstrates the EDS images of the B_4C/NRL flexible films. The small bright spots in the figure represent the B_4C particles, indicating that they are well distributed in the NRL. The number of small bright spots increased with the B_4C concentration. The main component of NRL is a kind of polyisoprene, and its molecular formula is $(C_5H_8)_n$. The main components of the B_4C/NRL flexible films are B_4C and NR. Accordingly, the main elements of the B_4C/NRL flexible films are B, C, and H. B and C can be detected using EDS; however, H cannot be detected using EDS. Excluding the weight of H, the weights of B and C in B_4C/NRL obtained using EDS are presented in Table 2. The mass fraction of B in B_4C is 0.7826. The mass

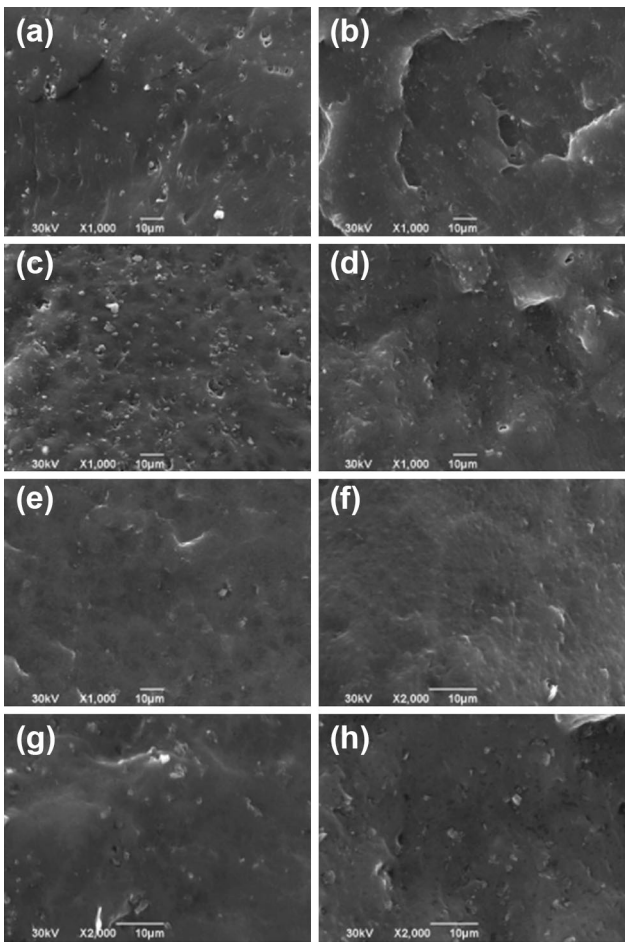

Fig. 3 SEM images of B_4C/NRL flexible films with **a** 5 wt%, **b** 10 wt%, **c** 15 wt%, **d** 20 wt%, **e** 25 wt%, **f** 35 wt%, **g** 45 wt%, and **h** 55 wt% B_4C

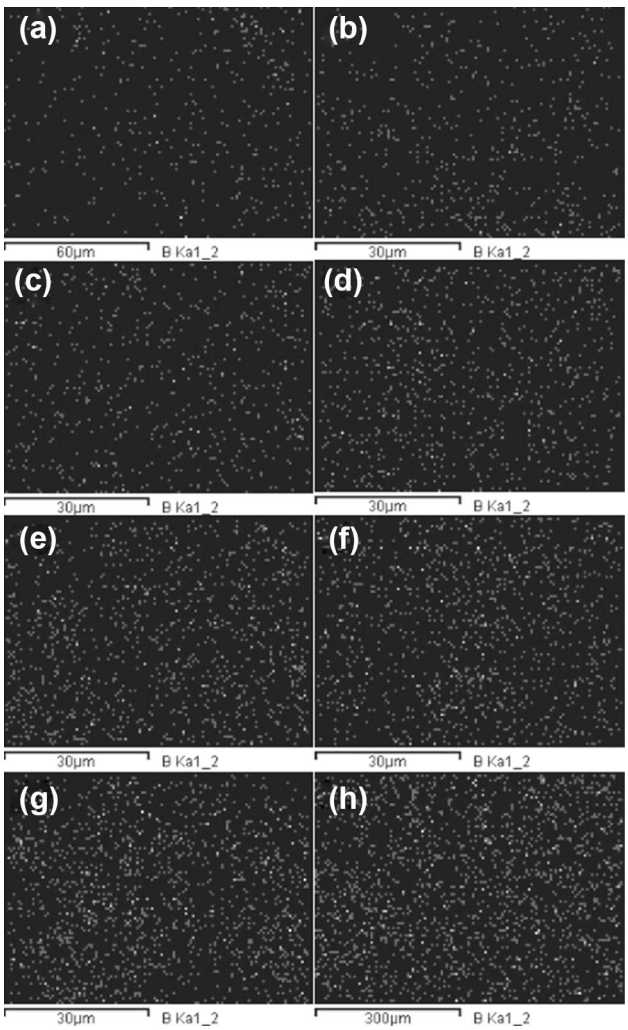

Fig. 4 EDS images of B_4C/NRL flexible films with **a** 5 wt%, **b** 10 wt%, **c** 15 wt%, **d** 20 wt%, **e** 25 wt%, **f** 35 wt%, **g** 45 wt%, and **h** 55 wt% B_4C

Table 2 Quantitative analysis data of B_4C/NRL from EDS

Designed content of B_4C (wt%)	5	10	15	20	25	35	45	55
B Kα (wt%)	4.19	8.42	12.09	16.39	19.99	27.91	35.26	42.93
C Kα (wt%)	95.81	91.58	87.91	83.61	80.01	72.09	64.74	57.07
Total (wt%)	100	100	100	100	100	100	100	100
Calculated content of B_4C (wt%)	5.35	10.75	15.45	20.94	25.54	35.66	45.05	54.86
Calculated content of NR (wt%)	94.65	89.25	84.55	79.06	74.46	64.34	54.95	45.14
Total (wt%)	100	100	100	100	100	100	100	100

fraction of B_4C in B_4C/NRL is calculated by dividing 0.7826 by the weight of B. In Table 2, the designed contents of B_4C are consistent with the calculated values.

The SEM images of the outside and inside surfaces of the B_4C/NRL flexible films are shown in Fig. 5. The inside surface is defined as the film face adjacent to the mold during dipping. The outside surface is defined as the film face away from the mold during dipping. Both the inside and outside surfaces were smooth, and no apparent particles peeled from the matrix. This indicates that the surface of the film is in a good condition and conducive to practical applications.

3.2 WAXD of the B_4C/NRL films

The WAXD patterns of the B_4C/NRL flexible films are presented in Fig. 6. The peak observed at 20° revealed the amorphous feature of NR (Fig. 6a). The strongest peak of B_4C was observed at 37.6° (Fig. 6a). The peak amplitude at 20° became weakened with an increase of B_4C (Fig. 6b), and thus, the relative peak amplitude (i.e., the ratio of peak amplitudes at 37.6°/20°) improved (Fig. 6b). The WAXD feature of NRL became weaker with an increase in the concentration of B_4C, whereas the WAXD feature of B_4C became stronger. When the content of B_4C was in the range

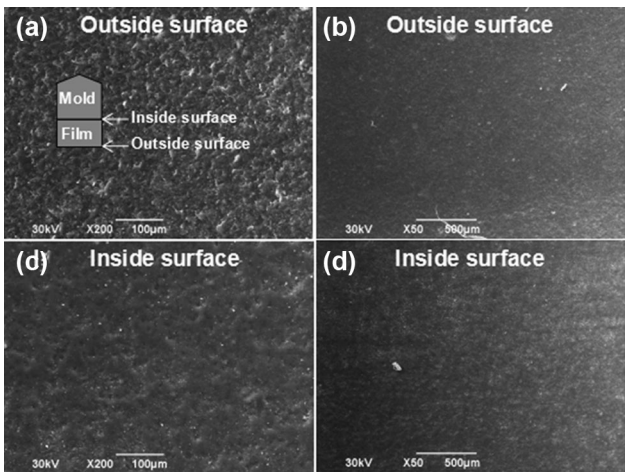

Fig. 5 SEM images of the outside surface **a**, **b** and inside surface **c**, **d** of a B_4C/NRL flexible film containing 25 wt% B_4C

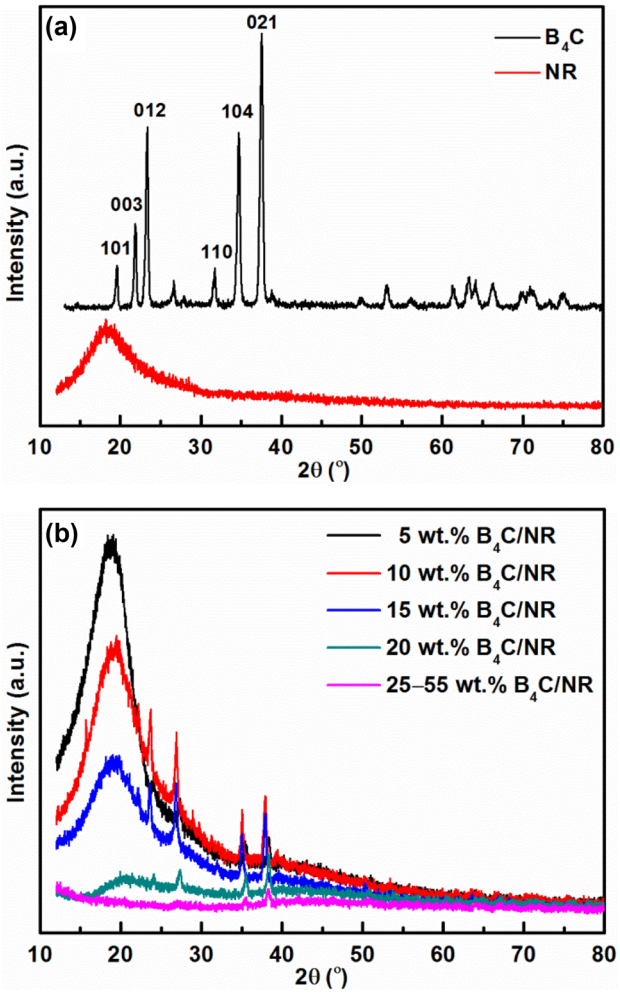

Fig. 6 (Color online) WAXD pattern of **a** B_4C and NRL, and **b** B_4C/NRL flexible films

of 25–55 wt%, the WAXD pattern of the B_4C/NRL flexible films was weak.

3.3 FT-IR of B_4C/NRL films

The FT-IR spectra of the B_4C/NRL flexible films are shown in Fig. 7. The addition of B_4C did not change the peak position of the IR characteristic peak of NRL, indicating that B_4C did not change the molecular structure of

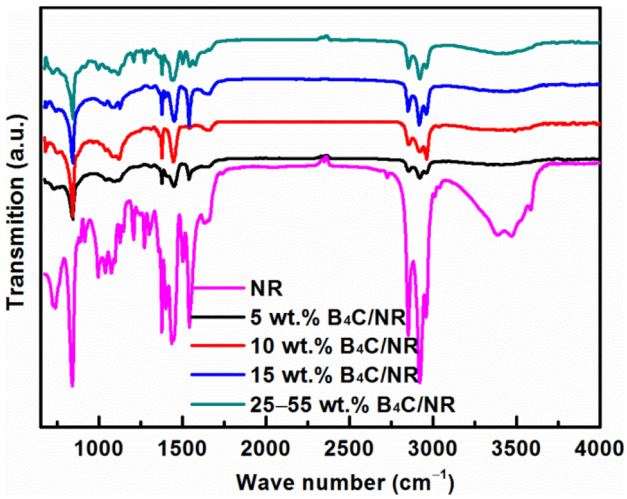

Fig. 7 (Color online) FT-IR spectra of the B_4C/NRL flexible films

NRL. The wave numbers of the B_4C/NRL composite are summarized in Table 3. Our results are consistent with the previous reports of IR spectra of NR illustrated as follows: The wave number of nearly 3500 cm^{-1} was attributed to the N–H stretching from a small amount of protein in the NR. The protein content decreased after curing in boiling water and subsequent washing. Therefore, the corresponding peak was not apparent in the B_4C/NRL films. The wave numbers of 2966 and 2913 cm^{-1} were attributed to the C–H stretching [27], whereas the wave numbers of 2846, 1665, and 1438 cm^{-1} corresponded to the C–H stretching, C=C stretching, and CH_2 deformation, respectively [28]. The wave numbers of 1535 and 1076 cm^{-1} were attributed to the O–H bending and C–C stretching, respectively [29]. The wave number of 1380 cm^{-1} was attributed to the CH_3 bending [30]. The wave numbers of 1665 and 836 cm^{-1} were attributed to the C=C stretching and C=C bending of the isoprene unit, respectively [31].

3.4 Mechanical property of B_4C/NRL films

B_4C/NRL flexible films with 5, 10, 15, 20, 25, 35, 45, and 55 wt% B_4C were vulcanized by boiled water at 100 °C for 40, 60, or 80 min. The mechanical properties are illustrated in Fig. 8. The minimum tensile strength of all the samples was greater than 12 MPa (Fig. 8a), which is higher than that of the reported rubber for thermal neutron shielding [19–23]. The tensile strength of the 10% B_4C/NRL film was the highest under different vulcanizing temperatures. The tensile strength was the highest when films with different contents of B_4C were vulcanized for 60 min. The highest tensile strength among all the samples was 29 MPa. When considering the resulting strength and energy consumption, curing for 60 min was considered the optimal timeframe. As the B_4C concentration increased, the tensile strength of the B_4C/NRL films initially increased and thereafter decreased. The tensile strengths of the 5, 10, and 15 wt% B_4C/NRL films were greater than that of the NRL film. The tensile strengths of the 20, 25, 35, 45, and 55 wt% B_4C/NRL films were less than that of the NRL film. No other fillers were added to NRL as reinforcing agents. The added B_4C played the role of a reinforcing agent in the NRL. The addition of 10 wt% B_4C achieved the best reinforcing effect.

The elongation at break of the B_4C/NRL films did not vary significantly in the range of 600–810% (Fig. 8b), which is higher than that of the reported rubber for thermal neutron shielding [19–23], indicating that the B_4C/NRL films are suitable for the high elasticity requirement in some cases, such as gloves.

Figure 9 shows the hardness of the B_4C/NRL films. The shore hardness of the B_4C/NRL films increased with the increase in concentration of B_4C; however, the B_4C/NRL films were still flexible for practical applications in comparison with common latex gloves. The hardness is lower than that of the reported rubber for thermal neutron shielding [24].

3.5 Thermal neutron shielding property of B_4C/NRL films

The density of the B_4C/NRL film was calculated using the following equation:

$$\rho = \frac{m_1 + m_2}{v_1 + v_2} = \frac{\rho_2/x_2}{\rho_2 \cdot x_1/(\rho_1 \cdot x_2) + 1}, \quad (4)$$

where m, v, ρ, and x represent the mass, volume, density, and mass fraction, respectively, and subscripts 1 and 2 represent B_4C and NRL, respectively. Thus, $m_1/m_2 = x_1/x_2 = \rho_1 v_1/\rho_2 v_2$, and $x_1 + x_2 = 1$. The density of NRL measured using the Archimedes principle was 1 g cm^{-3}. The density of the B_4C/NRL flexible film is shown in Fig. 10. The experimental values are consistent with the calculated values.

Analogous with the attenuation for γ-rays, the mass attenuation coefficient of the B_4C/NRL composite was calculated using the following equation [7, 32]:

Table 3 Wave numbers of the peaks in the FT-IR spectra of the B_4C/NRL films

ν (cm^{-1})	2966	2913	2846	1665	1535	1438	1380	1076	839
Vibration mode	ν (C–H)	ν (C–H)	ν (C–H)	ν (C=C)	δ (O–H)	δ (CH_2)	δ (CH_3)	ν (C–C)	δ (C=C)

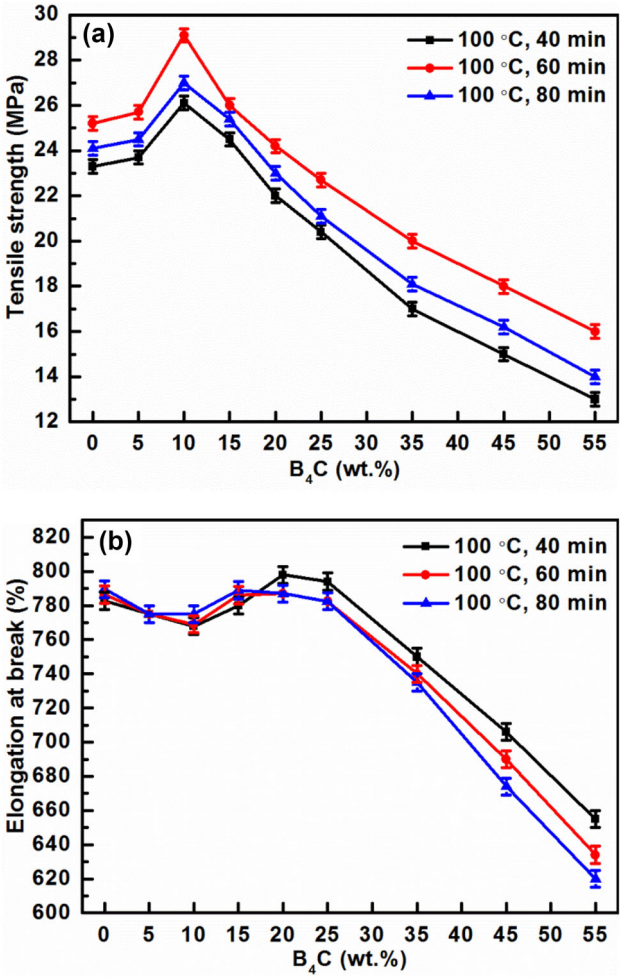

Fig. 8 (Color online) Tensile strength **a** and elongation at break **b** of the B_4C/NRL flexible films

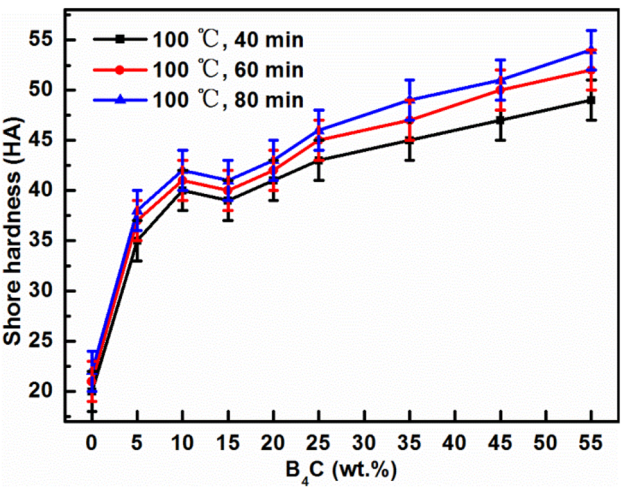

Fig. 9 (Color online) Shore hardness of the B_4C/NRL flexible films

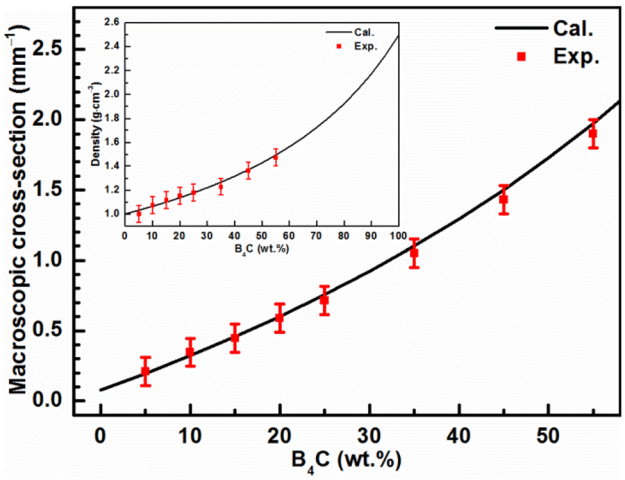

Fig. 10 (Color online) Macroscopic cross-section of the B_4C/NRL flexible films for attenuating thermal neutrons. Inset image: Density of the B_4C/NRL flexible films

$$\frac{\sigma}{\rho} = \sigma_{\mathrm{m}} = \sigma_{\mathrm{m},1} \cdot x_1 + \sigma_{\mathrm{m},1} \cdot x_2, \tag{5}$$

where σ is the line attenuation coefficient or macroscopic cross-section of the composite; σ_{m} is the mass attenuation coefficient of the B_4C/NRL composite; the terms $\sigma_{\mathrm{m},1}$ and $\sigma_{\mathrm{m},2}$ represent the mass attenuation coefficients of B_4C and NR, respectively. The mass attenuation coefficient of B_4C for attenuating thermal neutrons can be obtained from Monte Carlo simulations or the literature database. The macroscopic cross-section of B_4C for thermal neutrons (0.0253 eV) fitted by an experiment was 58.537 cm^{-1} [33]. As NR and high-density polyethylene (HDPE) are both mainly composed of carbon and hydrogen, the macroscopic cross-section of NR for attenuating thermal neutrons (0.0253 eV) was approximately equal to that of HDPE, which was determined by an experiment as 0.77 cm^{-1} [34].

The macroscopic cross-section of the B_4C/NRL composite was calculated using the following equation:

$$\sigma = (\sigma_{\mathrm{m},1} \cdot x_1 + \sigma_{\mathrm{m},2} \cdot x_2) \cdot \frac{\rho_2/x_2}{\rho_2 \cdot x_1/(\rho_1 \cdot x_2) + 1}. \tag{6}$$

The macroscopic cross-section of the B_4C/NRL flexible films for attenuating thermal neutrons is shown in Fig. 10. The experimental values of σ were obtained from Eq. (3). The experimental values and the values calculated using Eq. (6) are consistent with each other. However, our results are different from those in the literature [35]. This was mainly because our calculations of the macroscopic cross-section were based on experiments with thermal neutrons of energy 0.0253 eV. The most probable energy of thermal neutrons in the literature was larger than 0.0253 eV. [35].

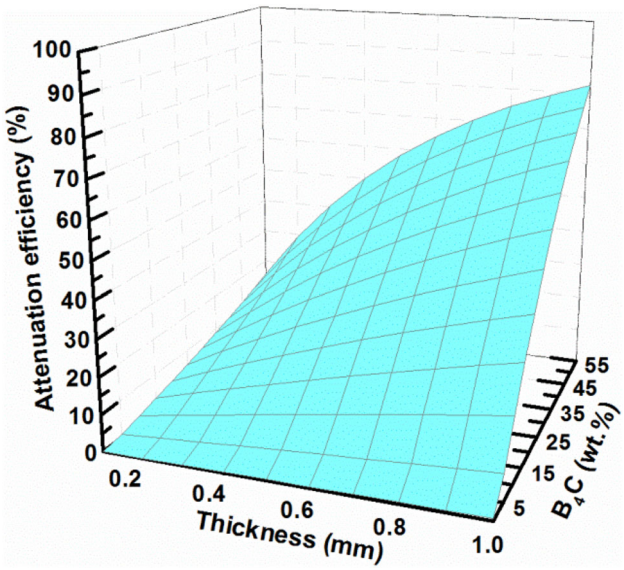

Fig. 11 (Color online) Shielding efficiency of the B_4C/NRL flexible films for attenuating thermal neutrons

After the macroscopic cross-section of the B_4C/NRL flexible films was obtained, the attenuation efficiency of the B_4C/NRL flexible films for thermal neutrons was calculated for different thicknesses and percentages of B_4C using Eq. (3). Figure 11 illustrates the attenuation efficiency of the B_4C/NRL flexible films for attenuating thermal neutrons (0.0253 eV). This result is favorable to engineering design. If the attenuation efficiency is set, suitable thickness and B_4C content can be designed to satisfy the attenuation efficiency. For a B_4C/NRL flexible film, the B_4C content can be calculated by measuring its density and thickness, which is easy to measure; subsequently, the efficiency for attenuating thermal neutrons (0.0253 eV) can be obtained.

4 Conclusion

B_4C/NRL flexible films for thermal neutron shielding were successfully prepared via dip-molding with B_4C content in the range of 5–55 wt%. The results indicate that B_4C was well dispersed in NRL. The stability of pre-vulcanized latex containing B_4C was satisfactory for practical applications. Both the inside and outside surfaces of the film were smooth.

The minimum elongation at break of the B_4C/NRL flexible films was greater than 600%; the minimum tensile strength of the B_4C/NRL flexible films was greater than 12 MPa; the hardness of the B_4C/NRL flexible films was in the range of 35–55 HA. These results indicate that the B_4C/NRL flexible films are flexible for practical applications.

The experimental and calculated values of the macroscopic cross-section of the B_4C/NRL flexible films were consistent with each other. The attenuation efficiency of the B_4C/NRL flexible films for thermal neutrons was calculated for different thicknesses and percentages of B_4C. The B_4C/NRL flexible films exhibited good attenuation effect for thermal neutrons. This result is favorable to engineering design. If the attenuation efficiency is set, suitable thickness and B_4C content can be designed to satisfy the attenuation efficiency.

References

1. D. Mendelsohn, J. Strelzow, N. Dea et al., Patient and surgeon radiation exposure during spinal instrumentation using intraoperative computed tomography-based navigation. Spine J. **16**, 343–354 (2016). https://doi.org/10.1016/j.spinee.2015.11.020
2. R. Madan, R. Benson, D.N. Sharma et al., Radiation induced heart disease: pathogenesis, management and review literature. J. Natl Cancer Inst. **27**, 187–193 (2015). https://doi.org/10.1016/j.jnci.2015.07.005
3. A.V. Mozhayev, R.K. Piper, B.A. Rathbone et al., Moderator design studies for a new neutron reference source based on the D-T fusion reaction. Radiat. Phys. Chem. **123**, 87–96 (2016). https://doi.org/10.1016/j.radphyschem.2016.02.004
4. M.H. Choopan, H. Khalafi, Y. Kasesaz et al., Design, construction and characterization of a new neutron beam for neutron radiography at the Tehran Research Reactor. Nucl. Instrum. Methods Phys. Res., Sect. A **818**, 1–8 (2016). https://doi.org/10.1016/j.nima.2016.02.040
5. J. Valentin, *The 2007 Recommendations of the International Commission on Radiological Protection* (Elsevier, Amsterdam, 2007)
6. I. Akkurt, A. Calik, H. Akyıldırım, The boronizing effect on the radiation shielding and magnetization properties of AISI 316L austenitic stainless steel. Nucl. Eng. Des. **241**, 55–58 (2011). https://doi.org/10.1016/j.nucengdes.2010.10.009
7. I. Akkurt, A.M. El-Khayatt, The effect of barite proportion on neutron and gamma-ray shielding. Ann. Nucl. Eng. **51**, 5–9 (2013). https://doi.org/10.1016/j.anucene.2012.08.026
8. A.M. El-Khayatt, I. Akkurt, Photon interaction, energy absorption and neutron removal cross section of concrete including marble. Ann. Nucl. Eng. **60**, 8–14 (2013). https://doi.org/10.1016/j.anucene.2013.04.021
9. T. Piotrowski, M. Mazgaj, A. Żak et al., Importance of atomic composition and moisture content of cement based composites in neutron radiation shielding. Procedia Eng. **108**, 616–623 (2015). https://doi.org/10.1016/j.proeng.2015.06.188
10. J.J. Park, S.M. Hong, M.K. Lee et al., Enhancement in the microstructure and neutron shielding efficiency of sandwich type of 6061Al–B_4C composite material via hot isostatic pressing. Nucl. Eng. Des. **282**, 1–7 (2015). https://doi.org/10.1016/j.nucengdes.2014.10.020
11. H.S. Chen, W.X. Wang, Y.L. Li et al., The design, microstructure and mechanical properties of B_4C/6061Al neutron absorber composites fabricated by SPS. Mater. Des. **94**, 360–367 (2016). https://doi.org/10.1016/j.matdes.2016.01.030
12. J. Kim, J. Jun, M.K. Lee, Particle size-dependent pulverization of B_4C and generation of B_4C/STS nanoparticles used for neutron

absorbing composites. Nucl. Eng. Technol. **46**, 675–680 (2014). https://doi.org/10.5516/NET.06.2014.015
13. M. Celli, F. Grazzi, M. Zoppi, A new ceramic material for shielding pulsed neutron scattering instruments. Nucl. Instrum. Methods Phys. Res., Sect. A **565**, 861–863 (2006). https://doi.org/10.1016/j.nima.2006.05.234
14. S.I. Tadadjeu, B.D. Ngom, M. Msimanga et al., Coatings synthesised by the pulsed laser ablation of a B_4C/W_2B_5 ceramic composite. Thin Solid Films **593**, 5–9 (2015). https://doi.org/10.1016/j.tsf.2015.09.030
15. D. Sarıyer, R. Küçer, N. Küçer, Neutron shielding properties of concretes containing boron carbide and Ferro–Boron. Procedia Soc. Behav. Sci. **195**, 1752–1756 (2015). https://doi.org/10.1016/j.sbspro.2015.06.320
16. I. Akkurt, R. Altindag, K. Gunoglu et al., Photon attenuation coefficients of concrete including marble aggregates. Ann. Nucl. Eng. **43**, 56–60 (2012). https://doi.org/10.1016/j.anucene.2011.12.031
17. I. Akkurt, H. Akyıldırım, B. Mavi et al., Photon attenuation coefficients of concrete includes barite in different rate. Ann. Nucl. Eng. **37**, 910–914 (2010). https://doi.org/10.1016/j.anucene.2010.04.001
18. J. Jun, J. Kim, Y. Bae et al., Enhancement of dispersion and adhesion of B_4C particles in epoxy resin using direct ultrasonic excitation. J. Nucl. Mater. **416**, 293–297 (2011). https://doi.org/10.1016/j.jnucmat.2011.06.014
19. H. Chai, X.B. Tang, M.X. Ni et al., Preparation and properties of flexible flame-retardant neutron shielding material based on methyl vinyl silicone rubber. J. Nucl. Mater. **464**, 210–215 (2015). https://doi.org/10.1016/j.jnucmat.2015.04.048
20. T. Özdemir, İ.K. Akbay, H. Uzun et al., Neutron shielding of EPDM rubber with boric acid: mechanical, thermal properties and neutron absorption tests. Prog. Nucl. Energy **89**, 102–109 (2016). https://doi.org/10.1016/j.pnucene.2016.02.007
21. T. Özdemir, A. Güngör, İ.A. Reyhancan, Flexible neutron shielding composite material of EPDM rubber with boron trioxide: mechanical, thermal investigations and neutron shielding tests. Radiat. Phys. Chem. **131**, 7–12 (2017). https://doi.org/10.1016/j.radphyschem.2016.10.012
22. S.E. Gwaily, M.M. Badawy, H.H. Hassan et al., Natural rubber composites as thermal neutron radiation shields: I. B_4C/NR composites. Polym. Test. **21**, 129–133 (2002). https://doi.org/10.1016/S0142-9418(01)00058-7
23. S.E. Gwaily, M.M. Badawy, H.H. Hassan et al., Influence of thermal aging on crosslinking density of boron carbide/natural rubber composites. Polym. Test. **22**, 3–7 (2003). https://doi.org/10.1016/S0142-9418(02)00024-7
24. K. Ninyong, E. Wimolmala, N. Sombatsompop et al., Potential use of NR and wood/NR composites as thermal neutron shielding materials. Polym. Test. **59**, 336–343 (2017). https://doi.org/10.1016/j.polymertesting.2017.02.020
25. S. Norhazariah, A.R. Azura, R. Sivakumar et al., Effect of different preparation methods on crosslink density and mechanical properties of carrageenan filled natural rubber (NR) latex films. Procedia Chem. **19**, 986–992 (2016). https://doi.org/10.1016/j.proche.2016.03.146
26. R. Adeli, S.P. Shirmardi, S.J. Ahmadi, Neutron irradiation tests on B_4C/epoxy composite for neutron shielding application and the parameters assay. Radiat. Phys. Chem. **127**, 140–146 (2016). https://doi.org/10.1016/j.radphyschem.2016.06.026
27. Y.S. Lee, W.K. Lee, S.G. Cho et al., Quantitative analysis of unknown compositions in ternary polymer blends: a model study on NR/SBR/BR system. J. Anal. Appl. Pyrolysis **78**, 85–94 (2007). https://doi.org/10.1016/j.jaap.2006.05.001
28. S.A. Riyajan, S. Chaiponban, K. Tanbumrung, Investigation of the preparation and physical properties of a novel semi-interpenetrating polymer network based on epoxised NR and PVA using maleic acid as the crosslinking agent. Chem. Eng. J. **153**, 199–205 (2009). https://doi.org/10.1016/j.cej.2009.05.043
29. E.A. Dil, M. Ghaedi, A.M. Ghaedi et al., Modeling of quaternary dyes adsorption onto ZnO–NR–AC artificial neural network: analysis by derivative spectrophotometry. J. Ind. Eng. Chem. **34**, 186–197 (2016). https://doi.org/10.1016/j.jiec.2015.11.010
30. D. Yuan, K. Chen, C. Xu et al., Crosslinked bicontinuous bio-based PLA/NR blends via dynamic vulcanization using different curing systems. Carbohydr. Polym. **113**, 438–445 (2014). https://doi.org/10.1016/j.carbpol.2014.07.044
31. S. Amnuaypanich, J. Patthana, P. Phinyocheep, Mixed matrix membranes prepared from natural rubber/poly(vinyl alcohol) semi-interpenetrating polymer network (NR/PVA semi-IPN) incorporating with zeolite 4A for the pervaporation dehydration of water–ethanol mixtures. Chem. Eng. Sci. **64**, 4908–4918 (2009). https://doi.org/10.1016/j.ces.2009.07.028
32. S.A.M. Issa, Effective atomic number and mass attenuation coefficient of PbO–BaO–B_2O_3 glass system. Radiat. Phys. Chem. **120**, 33–37 (2016). https://doi.org/10.1016/j.radphyschem.2015.11.025
33. L. Zhang, J.M. Shi, X. Lian et al., Neutron absorption properties of Al-B_4C composite materials. Mater. Rev. **30**, 21–30 (2016). https://doi.org/10.11896/j.issn.1005-023x.2016.16.005. **(in Chinese)**
34. Y.H. Liu, Y. Zhi, J.C. Zuo et al., Research on enhance of polyethylene composite and its thermal neutron shielding performance by borate whisker. At. Energy Sci. Technol. **49**, 349–353 (2015). https://doi.org/10.7538/yzk.2015.49.02.0349
35. Z. Soltani, A. Beigzadeh, F. Ziaie et al., Effect of particle size and percentages of Boron carbide on the thermal neutron radiation shielding properties of HDPE/B4C composite: experimental and simulation studies. Radiat. Phys. Chem. **127**, 182–187 (2016). https://doi.org/10.1016/j.radphyschem.2016.06.027